

# Analysis of Vehicle Longitudinal Dynamics during Acceleration and Braking Events

Renan Koji Minakawa Fujii, Sergio Junichi Idehara

**Abstract**— The suspension system is a critical component in vehicle dynamics and stability, particularly as pitch rotation redistributes vehicle weight between axles, affecting tire-road friction limits. This study examines the longitudinal dynamic behavior of a vehicle under varying acceleration and braking conditions. A seven-degree-of-freedom numerical model was developed, focusing on vertical movements. Empirical suspension parameters and center of gravity positions were used as input, and dynamic tests with an instrumented vehicle provided acceleration and pitch angle data for validation. Results showed that the pitch angle of the sprung mass reached  $-0.5^\circ$  during acceleration and  $1.0^\circ$  during braking, both with and without ABS. Additionally, modal analysis identified vibration modes that contributed the most to pitch motion, with a natural frequency of approximately 1.5 Hz for one of the dominant pitch modes.

**Index Terms**—Vehicle dynamics, suspension system, pitch angle, numerical simulation

## I. INTRODUCTION

A significant portion of the study and resources is dedicated to developing the suspension system, aiming to provide a component that is safe, comfortable, and reliable. The suspension absorbs road irregularities and transfers these forces to the sprung mass. Therefore, it directly influences passenger comfort by determining the vibration modes experienced by the sprung mass. Additionally, it enhances vehicle safety and stability by maintaining tire-road contact. According to [1], substantial investment is necessary to balance comfort, safety, and performance. The vehicle must handle cornering, acceleration, and braking with roll and pitch values that keep all wheels in contact with the ground, while preserving drivability. Classical mechanics principles are applied to vehicle dynamics to design system components and understand vehicle behavior.

For longitudinal dynamics, the focus is on evaluating the movement caused by forces during acceleration and braking. The vehicle has one degree of freedom for pitch rotation (around the y-axis) and one degree of freedom for translation along the x-axis. As noted in [2], variations in longitudinal acceleration lead to changes in the normal load on the vehicle's axles, affecting the suspension spring length. During braking, the force acts at the vehicle's center of gravity, generating a rotational moment around the pitch center.

Modeling the pitch movement of a vehicle is important for understanding vehicle stability and performance, as noted in studies such as [3]. The pitch angle affects traction, braking efficiency, and overall vehicle control. For example,

Renan Koji Minakawa Fujii, Mobility Engineering Department, Federal University of Santa Catarina, Joinville, Brazil.

Sergio Junichi Idehara, Mobility Engineering Department, Federal University of Santa Catarina, Joinville, Brazil.

acceleration often causes a forward tilt (squat), while braking induces a backward tilt (dive). These dynamics have implications for vehicle safety and handling. By using both numerical and experimental methods, researchers can simulate pitch behavior, enabling improvements in suspension systems and longitudinal dynamic controls.

Models using sensor fusion techniques with accelerometer, gyroscope, and magnetometer data are commonly employed to estimate vehicle pitch angles during dynamic tests [4]. These models provide a more accurate representation of real-world driving conditions, where pitch angles can vary significantly due to factors like road surface and load conditions. Researchers have worked extensively on improving the precision of these models by incorporating data from multi-sensor systems such as inertial measurement units (IMUs) and vehicle dynamics models. For instance, the work of [5] demonstrates how six-dimensional IMU data can be combined with wheel speed and steering angle sensors to estimate pitch and roll angles, thereby refining the understanding of vehicle attitudes during transient and steady-state conditions. Similarly, other studies have used techniques like sensor fusion and Kalman filtering to enhance the accuracy of pitch angle estimation during braking and acceleration.

The work of [6] demonstrated the importance of accurate pitch movement analysis in real driving conditions, linking dynamic pitch behavior to vehicle performance on different road surfaces. Additionally, [7] used image processing techniques to analyze pitch dynamics in agricultural tractors, highlighting the role of tire compression and cabin oscillations in determining vehicle stability during braking. These findings are applied for developing robust models that account for real-world variability in pitch movement. In modern vehicles, typical pitch angles during heavy braking can range from  $0.5^\circ$  to  $1.5^\circ$ , as observed in studies on commercial vehicles [8]. When compared with a vehicle's natural frequencies, particularly those associated with the pitch axis, these angles may coincide with critical oscillation frequencies, amplifying the dynamic response if not properly controlled. Moreover, pitch frequency, which usually falls between 1 and 2 Hz, plays a role in ride comfort, as higher frequencies can lead to passenger discomfort and reduced stability [9].

During hard braking, as observed in various experimental studies, such as those involving ABS and regenerative braking systems [10][11], the pitch angle reached  $1.5^\circ$ . For instance, regenerative braking systems can complicate pitch dynamics due to the interaction between mechanical and electronic braking. Understanding these dynamics helps improve vehicle handling, particularly in high-performance vehicles or those subjected to frequent braking and acceleration. Accurate modeling of this behavior supports the design of advanced control systems that mitigate

excessive pitch and enhance vehicle performance, as explored by [11].

Reference [12] highlighted the importance of coupling longitudinal and vertical dynamics when vehicles encounter uneven road surfaces. Their study demonstrated that vertical dynamics affect not only vehicle comfort but also powertrain efficiency, particularly under off-road conditions. Similarly, [13] emphasized the need to consider the interaction between vertical, longitudinal, and roll dynamics in heavy-duty vehicles to understand how these forces influence overall vehicle performance. These studies emphasize the value of modeling vehicle dynamics comprehensively, accounting for multiple axes of motion that impact stability.

In commercial vehicle applications, pitch angles often vary between  $0.5^\circ$  and  $2^\circ$  during intense braking maneuvers [12], and precise control of these movements can enhance vehicle performance. As noted in [14], large trucks can experience pitch angles of up to  $1.5^\circ$  to  $2.0^\circ$  during braking, with even greater variations observed in off-road environments. The challenge is to accurately predict these dynamics in different driving scenarios, as vehicles respond to both internal factors, such as suspension stiffness and mass distribution, and external conditions, like road surface irregularities and vehicle accelerations.

Recent studies have investigated vehicle dynamics in detail using updated models and control systems to improve pitch stability. The work in [9] introduces a hydraulically interconnected suspension system that decouples roll and pitch modes, enhancing vehicle stability while maintaining ride comfort. This innovation is particularly useful in reducing pitch-induced discomfort, which is common in vehicles with a higher center of gravity, such as SUVs and heavy trucks. These systems offer improved pitch control, resulting in smoother transitions during braking and acceleration. In that study, each suspension assembly's displacement is influenced by a hydraulic cylinder, causing variations in suspension stiffness that directly affect pitch and roll movements. The pitch angle with the hydraulic system is reduced by approximately  $0.2^\circ$  compared to the vehicle's original configuration at the point of maximum inclination.

With the development of advanced suspension systems, such as magnetorheological (MR) dampers, the control of pitch movement has become more precise. These systems enable real-time adjustment of damping forces to minimize pitch and enhance vehicle stability during maneuvers like cornering and emergency braking [15]. The analyses and developments by [16] were driven by the increased use of driver assistance systems and autonomous driving technologies in commercial vehicles. These systems interpret signals from sensors that collect data on wheel rotation and the positioning of objects around the vehicle, triggering the steering and braking systems to influence the vehicle's trajectory.

This study aims to evaluate the pitch behavior of a vehicle under various acceleration and braking conditions. The focus is on developing a numerical model to simulate the vehicle's pitch response and validate it using experimental data. By comparing the simulated results with real-world measurements, the accuracy of the model and its potential

for optimizing vehicle performance can be assessed.

## II. METHODOLOGY

### A. Vehicle Numerical Model

The dynamic model developed for this study considers seven degrees of freedom: four for the unsprung mass and three for the vehicle body motion (pitch, roll, and vertical displacement), as illustrated in Fig. 1. The model equations were derived from classical mechanics, incorporating forces generated by the suspension system and the vehicle's mass distribution. Numerical integration using the Runge-Kutta method was employed to simulate the dynamic response over time for each degree of freedom (DOF).

Each wheel assembly has one degree of freedom for vertical displacement ( $z_n$ ,  $n \in \{1,2,3,4\}$ ). The sprung mass also has one degree of freedom for vertical displacement ( $z$ ) and two degrees of freedom for rotation: one around the x-axis ( $\phi$ ) and one around the y-axis ( $\theta$ ), which is the focus of this study.

The suspension force ( $F_n$ ) from the spring and damper can be described using the displacements of the unsprung mass ( $z_n$ ) and the sprung mass at the mounting points ( $z_{sn}$ ), along with their velocities ( $\dot{z}_n$  and  $\dot{z}_{sn}$ ). The spring stiffness is represented by  $k_n$ , and the damping coefficient by  $c_n$ .

$$F_n = k_n \cdot (z_{sn} - z_n) + c_n \cdot (\dot{z}_{sn} - \dot{z}_n) \quad (1)$$

The displacement of the sprung mass is described as a function of the inclinations generated by roll ( $\phi$ ) and pitch ( $\theta$ ) movements. The following equations represent the vertical displacements at the suspension mounting points.

$$z_{s1} = z + d_1 \cdot \phi - d_3 \cdot \theta \quad (2)$$

$$z_{s2} = z - d_2 \cdot \phi - d_3 \cdot \theta \quad (3)$$

$$z_{s3} = z - d_2 \cdot \phi + d_4 \cdot \theta \quad (4)$$

$$z_{s4} = z + d_1 \cdot \phi + d_4 \cdot \theta \quad (5)$$

Equation (1) can be rewritten for each suspension individually, with indices 1, 2, 3, and 4 representing the front left, front right, rear right, and rear left suspensions, respectively.

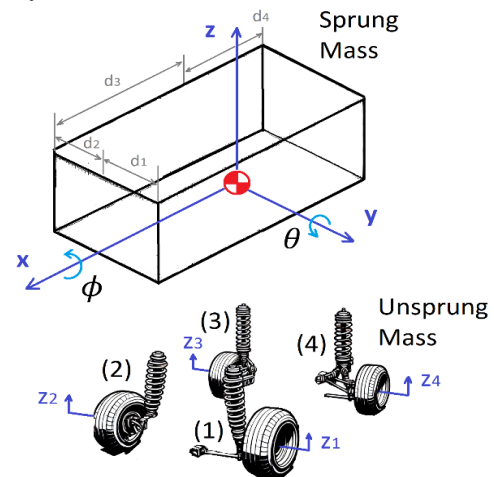


Figure 1 – Degrees of freedom of the unsprung and sprung masses.

$$F_1 = k_1(z + d_1 \cdot \phi - d_3 \cdot \theta) \quad (6)$$

$$+ c_1(\dot{z} + d_1 \cdot \dot{\phi} - d_3 \cdot \dot{\theta}) - k_1 \cdot z_1 - c_1 \cdot \dot{z}_1$$

$$F_2 = k_2(z - d_2 \cdot \phi - d_3 \cdot \theta) + c_2(\dot{z} - d_2 \cdot \dot{\phi} - d_3 \cdot \dot{\theta}) - k_2 \cdot z_2 - c_2 \cdot \dot{z}_2 \quad (7)$$

$$F_3 = k_3(z - d_2 \cdot \phi + d_4 \cdot \theta) + c_3(\dot{z} - d_2 \cdot \dot{\phi} + d_4 \cdot \dot{\theta}) - k_3 \cdot z_3 - c_3 \cdot \dot{z}_3 \quad (8)$$

$$F_4 = k_4(z + d_1 \cdot \phi + d_4 \cdot \theta) + c_4(\dot{z} + d_1 \cdot \dot{\phi} + d_4 \cdot \dot{\theta}) - k_4 \cdot z_4 - c_4 \cdot \dot{z}_4 \quad (9)$$

The force and moment balances acting on the sprung mass can be formulated for vertical displacement, rotation about the x-axis, and rotation about the y-axis, respectively:

$$M \cdot \ddot{z} = -F_1 - F_2 - F_3 - F_4 \quad (10)$$

$$I \cdot \ddot{\phi} = -F_1 \cdot d_1 + F_2 \cdot d_2 + F_3 \cdot d_1 - F_4 \cdot d_2 \quad (11)$$

$$J \cdot \ddot{\theta} = F_1 \cdot d_3 + F_2 \cdot d_3 - F_3 \cdot d_4 - F_4 \cdot d_4 + \tau_{exc} \quad (12)$$

Based on the previous equations, the differential equations for each degree of freedom of the sprung mass are as follows:

$$M \cdot \ddot{z} + \sum_{n=1}^{n=4} c_n \cdot (\dot{z} - \dot{z}_n) + \sum_{n=1}^{n=4} k_n \cdot (z - z_n) + (c_1 \cdot d_1 - c_2 \cdot d_2 - c_3 \cdot d_1 + c_4 \cdot d_2) \cdot \dot{\phi} + (-c_1 \cdot d_3 - c_2 \cdot d_3 + c_3 \cdot d_4 + c_4 \cdot d_4) \cdot \dot{\theta} + (k_1 \cdot d_1 - k_2 \cdot d_2 - k_3 \cdot d_1 + k_4 \cdot d_2) \cdot \phi + (-k_1 \cdot d_3 - k_2 \cdot d_3 + k_3 \cdot d_4 + k_4 \cdot d_4) \cdot \theta = 0 \quad (13)$$

$$I \cdot \ddot{\phi} - (c_1 \cdot d_1 - c_2 \cdot d_2 - c_3 \cdot d_1 + c_4 \cdot d_2) \cdot \dot{z} - (c_1 \cdot d_1^2 + c_2 \cdot d_2^2 + c_3 \cdot d_1 \cdot d_2 + c_4 \cdot d_1 \cdot d_2) \cdot \dot{\phi} - (-c_1 \cdot d_1 \cdot d_3 + c_2 \cdot d_2 \cdot d_3 - c_3 \cdot d_1 \cdot d_4 + c_4 \cdot d_2 \cdot d_4) \cdot \dot{\theta} - (-c_1 \cdot d_1 \cdot \dot{z}_1 + c_2 \cdot d_2 \cdot \dot{z}_2 + c_3 \cdot d_1 \cdot \dot{z}_3 - c_4 \cdot d_2 \cdot \dot{z}_4) - (k_1 \cdot d_1 - k_2 \cdot d_2 - k_3 \cdot d_1 + k_4 \cdot d_2) \cdot z - (k_1 \cdot d_1^2 + k_2 \cdot d_2^2 + k_3 \cdot d_1 \cdot d_2 + k_4 \cdot d_1 \cdot d_2) \cdot \phi - (-k_1 \cdot d_1 \cdot d_3 + k_2 \cdot d_2 \cdot d_3 - k_3 \cdot d_1 \cdot d_4 + k_4 \cdot d_2 \cdot d_4) \cdot \theta - (-k_1 \cdot d_1 \cdot z_1 + k_2 \cdot d_2 \cdot z_2 + k_3 \cdot d_1 \cdot z_3 - k_4 \cdot d_2 \cdot z_4) = 0 \quad (14)$$

$$J \cdot \ddot{\theta} + (-c_1 \cdot d_3 - c_2 \cdot d_3 + c_3 \cdot d_4 + c_4 \cdot d_4) \cdot \dot{z} + (-c_1 \cdot d_1 \cdot d_3 + c_2 \cdot d_2 \cdot d_3 - c_3 \cdot d_2 \cdot d_4 + c_4 \cdot d_1 \cdot d_4) \cdot \dot{\phi} + (c_1 \cdot d_3^2 + c_2 \cdot d_3^2 + c_3 \cdot d_4^2 + c_4 \cdot d_4^2) \cdot \dot{\theta} + (c_1 \cdot d_3 \cdot \dot{z}_1 + c_2 \cdot d_3 \cdot \dot{z}_2 - c_3 \cdot d_4 \cdot \dot{z}_3 - c_4 \cdot d_4 \cdot \dot{z}_4) + (-k_1 \cdot d_3 - k_2 \cdot d_3 + k_3 \cdot d_4 + k_4 \cdot d_4) \cdot z + (-k_1 \cdot d_1 \cdot d_3 + k_2 \cdot d_2 \cdot d_3 - k_3 \cdot d_2 \cdot d_4 + k_4 \cdot d_1 \cdot d_4) \cdot \phi + (k_1 \cdot d_3^2 + k_2 \cdot d_3^2 + k_3 \cdot d_4^2 + k_4 \cdot d_4^2) \cdot \theta + (k_1 \cdot d_3 \cdot z_1 + k_2 \cdot d_3 \cdot z_2 - k_3 \cdot d_4 \cdot z_3 - k_4 \cdot d_4 \cdot z_4) = \tau_{exc} \quad (15)$$

For the unsprung mass dynamics, the differential equation is:

$$m_n \cdot \ddot{z}_n = c_n \cdot (\dot{z}_{sn} - \dot{z}_n) + k_n \cdot (z_{sn} - z_n) \quad (16)$$

The numerical model described by equations (13) – (16) has 7 degrees of freedom (DOF) and was implemented in MATLAB, which receives acceleration ( $\ddot{x}$ ) values measured experimentally by an accelerometer. These values are used as input, in the form of torque ( $\tau_{exc}$ ), as described in equation (17), at the center of gravity of the developed model. The *ode45* integrator was used to obtain the numerical solution.

$$\tau_{exc} = h_{CG} \cdot m_s \cdot \ddot{x} \quad (17)$$

Where,  $h_{CG}$  is the height of the center of gravity, and  $m_s$  is the sprung mass.

The simulated pitch angle time signal was digitally filtered using a 4th-order Butterworth low-pass filter with a cutoff frequency of 0.6 Hz and a sampling rate of 1,000 Hz. The simulation signal was processed to be comparable with the experimental measurements, as the instrumentation used in the sensor fusion process already filters out high frequencies from the measured data.

### B. Experimental Setup

To assess the mass distribution of the test vehicle, the car was lifted using a hoist, and a scale was placed under each wheel. To ensure accuracy, the process was repeated three times, and the average of these three measurements was used. The obtained values are presented in Table I, with the total mass corresponding to the sum of all values.

The calculation of the center of gravity (CG) height was performed by tilting the car. To achieve this, a device attached to the lift was used to raise the rear axle of the vehicle by 15°, while the front wheels remained supported on the scale. Fig. 2 shows the condition of the vehicle during the measurements. The CG height was measured as 355.01 mm from the floor and 1,598.57 mm from the rear axle.

The procedure to determine the suspension characteristics involved fully supporting the car on scales, then slightly lifting the vehicle to decompress the suspension. To calculate suspension stiffness, the distance from the center

Table I – Mass distribution on the vehicle at static position.

Wheel	Weight (kg)
Front Right	376.40
Front Left	381.13
Rear Right	205.53
Rear Left	207.60
Total	1,170.66

of the wheel to the wheel well was measured. For tire stiffness, the distance from the surface of the scale to the lowest point of the wheel was measured.

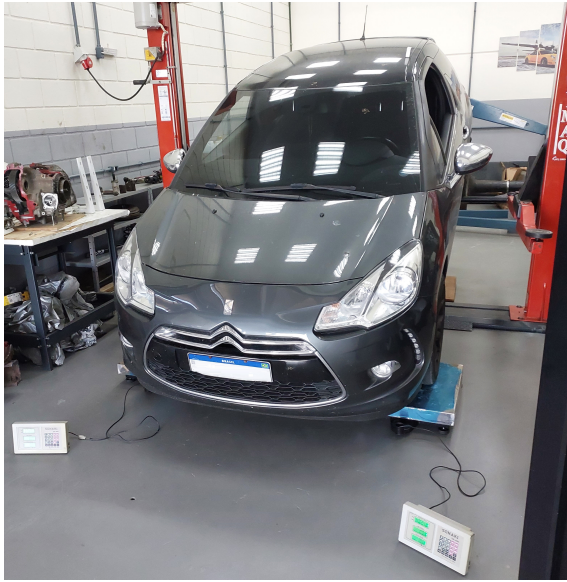


Figure 2 – Vehicle setup for center of gravity (CG) measurement, showing the rear axle raised by 15° while the front wheels remain supported on scales.

The resulting stiffness values are presented in Table II. The damping coefficients of each suspension were adjusted by comparing the time signal from the measured and simulated pitch responses.

Table II – Measured suspension and tire stiffness, and damping coefficients.

Component	Stiffness (N/m)	Damping (Ns/m)
Front Right Suspension	39,330.0	7770.0
Front Left Suspension	46,492.0	
Rear Right Suspension	33,062.0	15721.0
Rear Left Suspension	41,121.0	
Front Right Tire	466,820.0	0.0
Front Left Tire	361,980.0	
Rear Right Tire	266,620.0	
Rear Left Tire	180,600.0	

To estimate the rotational moments of inertia, the vehicle shape was approximated as a flat plate, and the resulting values are presented in Table III.

Table III – Approximated moment of inertia of the vehicle.

Axis	Mass Inertia Moment (kg.m <sup>2</sup> )
x-axis (I)	638.76
y-axis (J)	1992.57

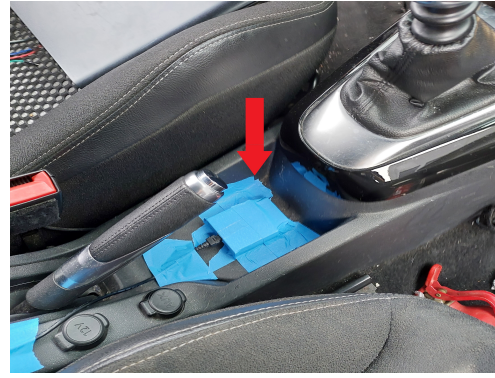


Figure 3 – Illustration of the installation position of the accelerometer and gyroscope, located near the handbrake.

A Citroën DS3 vehicle with 215 hp was instrumented with an accelerometer and gyroscope to capture data during acceleration and braking conditions. The instrumentation was carried out using the Freematics OBD-II board, equipped with an MPU-9250 sensor. The Putty software was used to receive and store the data. The sensor was positioned as close as possible to the vehicle's center of gravity, specifically mounted below the handbrake, as shown in Fig. 3.

The processed signal from the sensor data provides the vehicle inclination angles, calculated using sensor fusion for a more reliable measurement. In this case, accelerometer and gyroscope signals from the MPU-9250 were used. The data was filtered using a Kalman filter, which reduces noise in the measurements and provides a more stable result [17].

### C. Vehicular Experimental Test

The test was conducted on a straight path approximately 160 m long, located inside the Technological Center of Joinville (UFSC), as shown in Fig. 4. Measurements were taken with the vehicle starting from rest, accelerating fully to approximately 65–70 km/h, and then braking until coming to a complete stop. Several measurements were performed with and without the activation of the anti-lock braking system (ABS). For analysis, two runs were presented under the test conditions:

- Run 1 – The vehicle was accelerated at wide open throttle (WOT) and then braked with half force applied to the brake pedal;
- Run 2 – The vehicle was accelerated at wide open throttle (WOT) and then braked with full force applied to the brake pedal until the ABS was activated.

## III. RESULTS

This section describes the vibration modes and numerical model results obtained from the previous equations, which are excited by the measured acceleration signal. Additionally, a comparative analysis is performed between the model simulations and the experimental results.

### A. Modal Analysis

With the mass, stiffness, and damping matrices defined from equations (13) to (16), a harmonic solution can be used

to determine the natural frequencies and vibration modes. Through eigenvalue analysis, the vibration modes were obtained, as shown in Fig. 5. The natural frequency values are indicated above the figure. From these results, it is observed that the pitch degree of freedom exhibits the largest movement amplitude when excited in the first and second vibration modes.



Figure 4 – Vehicular test area with a length of 160 m.

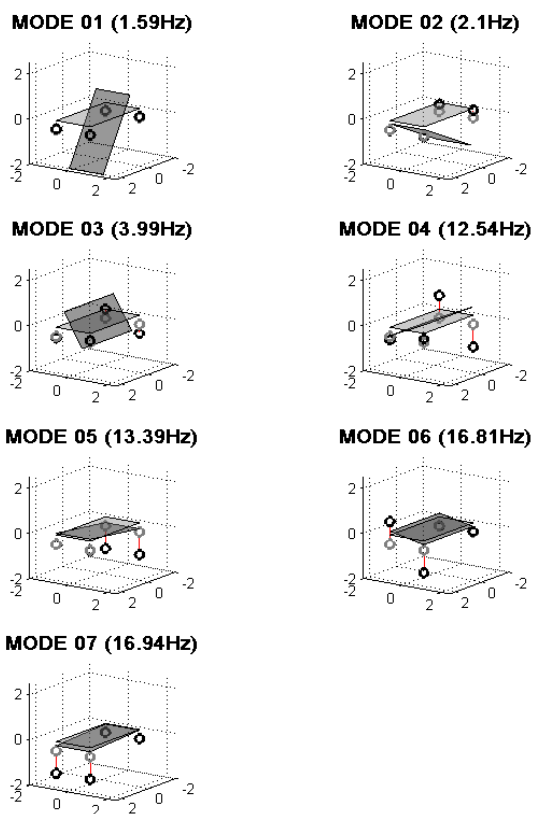


Figure 5 – Natural frequencies and vibration mode shapes of the vehicle with seven degrees of freedom.

In this case, the natural frequencies are 1.59 Hz and 2.10 Hz, respectively, which are the expected oscillation frequencies when measuring the pitch angle of the vehicle. The other vibration modes correspond to roll movement (mode 3) and unsprung mass vibrations (modes 4 to 7). These other modes are not considered in this study.

Fig. 6 presents the graphs of longitudinal acceleration and the pitch angle of the sprung mass during the test under Run 1 conditions. From these curves, the vehicle's behavior can be segmented into three distinct phases. In the first phase, the vehicle experiences an acceleration of approximately 5 m/s<sup>2</sup> for around 3 seconds.

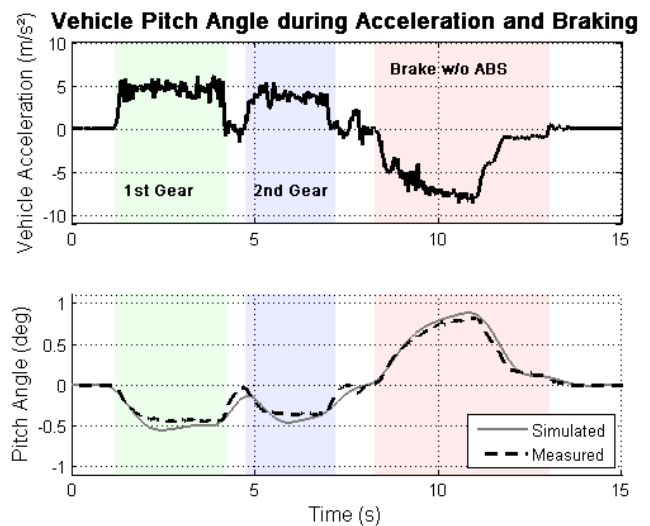


Figure 6 – Vehicle longitudinal acceleration and pitch angle for Run 1 (without ABS).

During this period, a squat movement is observed, with the sprung mass rotating by about  $-0.5^\circ$ . Next, the curves show a drop followed by a rise, indicating a gear shift. The second phase, between 4.7 seconds and 7.2 seconds, represents the acceleration and inclination values during second gear, highlighting the occurrence of a second squat movement.

In the final phase, braking occurs, with acceleration shifting from positive to negative values, reaching a maximum deceleration of approximately  $-8 \text{ m/s}^2$ . This event causes a dive movement, with the sprung mass rotating in the opposite direction and reaching a maximum inclination of about  $0.8^\circ$ . The vehicle's longitudinal displacement ends at 13.5 seconds. Immediately afterward, the sprung mass returns to its static equilibrium position. Observing the graphs, it is notable that the dashed black line (experimental data) and the gray line (simulated data) exhibit similar behavior in the pitch angle variation over time.

Fig. 7 shows the results of the same test procedure, but with ABS activated in Run 2. The vehicle accelerates from 1st to 3rd gear between 1.4 and 9.2 seconds, followed by strong braking to activate the ABS from 9.4 to 12.5 seconds. The deceleration reached  $-10.3 \text{ m/s}^2$ , with a maximum pitch angle of  $0.91^\circ$ . The simulated and experimental data show very similar results in terms of amplitude and the dynamic response of the vehicle's sprung mass.

Table IV presents a comparison of the maximum pitch angle amplitude between the measured and simulated signals. The percentage difference between the data is less than 13% for maximum inclination in both conditions, with and without ABS activation.

Table IV – Maximum pitch angle between simulated and experimental data.

Test	Pitch Angle Max.		Difference
	Experimental	Numerical	
Run 1	$0.80^\circ$	$0.89^\circ$	10.53%
Run 2	$0.91^\circ$	$1.03^\circ$	12.94%

To evaluate the accuracy of the numerical model, the root mean square error (RMSE) and mean square error (MSE) metrics were used as common performance measures.

Therefore, the model closely approximates the frequency components of the measured signal, with a percentage difference of 1.92%.

IV. CONCLUSION

The vehicle design process often uses predictive models of vehicle dynamics to enhance user safety and comfort. Additionally, current embedded systems in vehicles require the capability to estimate dynamic behavior in real-time to improve the performance of ADAS (Advanced Driver-Assistance Systems) and other vehicular subsystems. In this context, numerical models adjusted with real data from vehicle instrumentation are required for aiding automotive engineering and industry. To address this need, this paper developed a seven-degree-of-freedom model to predict the pitch angle of a vehicle during acceleration and braking. The comparison between the numerical model and experimental data demonstrates that the model can accurately predict pitch behavior in longitudinal dynamics, with a difference of less than 2% in natural frequency between the model and the measured signal. Future work will focus on refining the model by incorporating nonlinear suspension characteristics and the true height of the pitch center based on suspension geometry.

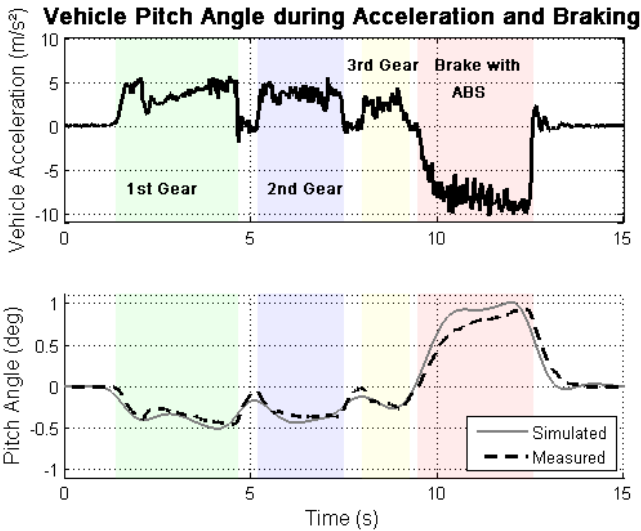


Figure 7 – Vehicle longitudinal acceleration and pitch angle for Run 2 (ABS activated).

These metrics are used to quantify the difference between the values predicted by the model and the actual observed values. The calculation can be performed using the following equation.

$$RMSE = \sqrt{MSE} = \sqrt{\frac{1}{n} \sum_{i=1}^n (y_i - p_i)^2} \quad (18)$$

Where  $n$  is the number of samples from the measurement,  $y_i$  is the model value for the pitch angle, and  $p_i$  is the experimentally measured value in the vehicle. The RMSE values for each test are shown in Table V.

The error values in the table are relatively low, less than  $0.1^\circ$ , compared to other RMSE results from [18], indicating a fair correlation between the signals from the numerical model and the measured data.

Table V – Mean squared error (MSE) and root mean square error (RMSE) between simulated and experimental pitch angle data.

Test	MSE	RMSE (°)
Run 1	0.0039	0.0627
Run 2	0.0069	0.0830

By plotting the time-frequency curve of the pitch rotation signal obtained in Run 1 using the spectrogram, the signal frequency can be observed, as shown in Fig. 8. Generally, the vehicle's highest suspension oscillation frequencies occur below 5 Hz. In the test, the largest amplitude of pitch rotation was observed around 1.56 Hz. When compared with the natural frequencies of the model obtained through modal analysis, the theoretical frequencies related to pitch were between 1.5 and 2.1 Hz (with the largest eigenvector amplitude corresponding to rotation around the y-axis).

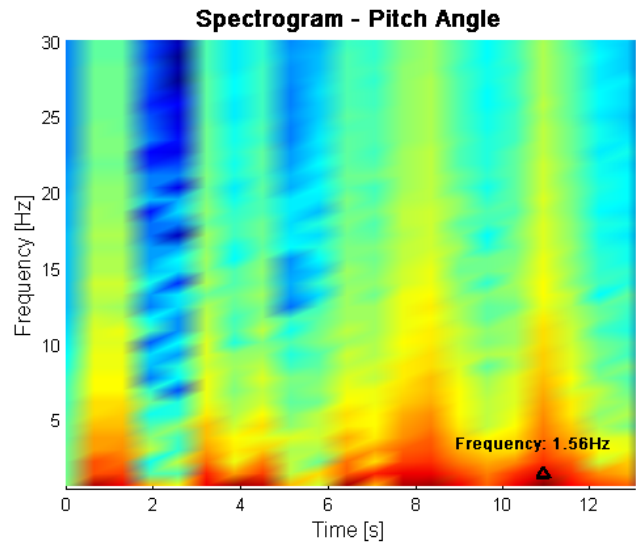


Figure 8 – Spectrogram of the measured pitch angle from Run 1 (Block size  $N = 128$ ,  $\Delta t = 0.01$  s).

REFERENCES

- [1] W. F. Milliken and D. L. Milliken, *Race Car Vehicle Dynamics*, SAE International, Warrendale, PA, p. 918,1994.
- [2] T. D. Gillespie, *Fundamentals of Vehicle Dynamics*, SAE International, Warrendale, PA, p. 520, 1992.
- [3] M.Tanelli, S. M. Savaresi, and A. Mergenthaler, "Dynamic coupling analysis between front and rear axle for abs systems design," *IFAC Proceedings Volumes*, vol. 40(10), 2007, pp. 375–382.
- [4] T. Massel, E. L. Ding, and M. Arndt, "Investigation of different techniques for determining the road uphill gradient and the pitch angle of vehicles," *Proceeding of the 2004 American Control Conference Boston, Massachusetts, June 30 - July 2, 2004*, pp. 2763–2768.
- [5] J. Oh and S. B. Choi, "Vehicle roll and pitch angle estimation using a cost-effective six-dimensional inertial measurement unit," *Proceedings of the IMechE Part D: Journal of Automobile Engineering*, vol. 227(4), pp. 577–590, 2013.
- [6] M. A. Abdullah, J. F. Jamil, and M. A. Salim, "Dynamic performances analysis of a real vehicle driving," *IOP Conference Series: Materials Science and Engineering*, vol. 100, pp. 1–10, 2015.

- [7] L. Onesto, M. Corno, and S. Savaresi, "Pitch dynamics analysis for an agricultural tractor with image processing validation through an off-board camera," *IFAC PapersOnLine*, vol. 52(5), pp. 492-497, 2019.
- [8] K. V. Subramaniam and S. C. Subramanian, "Impact of regenerative braking torque blend-out characteristics on electrified heavy road vehicle braking performance," *Vehicle System Dynamics*, vol. 59(2), pp. 269-294, 2021.
- [9] G. Xu, N. Zhang, and H. M. Roser, "Roll and pitch independently tuned interconnected suspension: Modelling and dynamic analysis," *Vehicle System Dynamics*, vol. 53(12), pp. 1830-1849, 2015.
- [10] R. S. Sharp, "Influences of suspension kinematics on pitching dynamics of cars in longitudinal manoeuvring," *Vehicle System Dynamics*, vol. 33, pp. 23-36, 1999.
- [11] D. Gowda, M. Ramesha, S. B. Sridhara, G. P. Naveena and K. P. Sachin, "Design of antilock braking system based on wheel slip estimation," *Journal of Physics: Conference Series*, vol. 1706, pp. 1-18, 2020.
- [12] Z. Guo, W. Wu, and S. Yuan, "Longitudinal-vertical dynamics of wheeled vehicle under off-road conditions," *Vehicle System Dynamics*, vol. 60(2), pp. 470-490, 2022.
- [13] Y. Li, S. Ma, K. Yu, and X. Guo, "Vehicle kinematic and dynamic modeling for three-axles heavy duty vehicle," *Mathematical Modelling and Control*, vol. 2(4), pp. 176-184, 2022.
- [14] D. G. Rideout, "Simulating coupled longitudinal, pitch and bounce dynamics of trucks with flexible frames," *Modern Mechanical Engineering*, vol. 2, pp. 176-189, 2012.
- [15] P. Krauze, and J. Kasprzyk, "Driving safety improved with control of magnetorheological dampers in vehicle suspension," *Appl. Sci.*, vol. 10, 2020, pp. 1-29.
- [16] C. Kurz, L. Stangenberg, and F. Gauterin, "A generic approach to modeling vehicle pitch dynamics on a vehicle test bench," *IEEE Open Journal of Vehicular Technology*, vol. 4, pp. 739-748, 2023.
- [17] D. Santana, C. Furukawa, and N. Maruyama, "Sensor fusion with low-grade inertial sensors and odometer to estimate geodetic coordinates in environments without GPS signal," *IEEE Latin America Transactions*, vol. 11, pp. 1015-1021, 2013.
- [18] H. Yang, J. Zhou, and Z. Qi, "Prediction model of pitch angle of greenhouse electric tractors based on time series analysis," *DYNA - Ingeniería e Industria*, vol. 98, (6), pp. 620-626, 2023